Letter

Anti-$\mathcal{PT}$ flatbands

Arindam Mallick,[1,*] Nana Chang,[1,2,3,†] Alexei Andreanov,[1,4,‡] and Sergej Flach[1,4,§]

[1]*Center for Theoretical Physics of Complex Systems, Institute for Basic Science (IBS), Daejeon 34126, Korea*

[2]*Beijing National Research Center for Information Science and Technology, Tsinghua University, Beijing 100084, China*

[3]*Center for Advanced Quantum Studies, Department of Physics, Beijing Normal University, Beijing 100875, People's Republic of China*

[4]*Basic Science Program, Korea University of Science and Technology (UST), Daejeon 34113, Korea*

(Received 23 August 2021; revised 7 December 2021; accepted 27 January 2022; published 28 February 2022)

We consider tight-binding single-particle lattice Hamiltonians which are invariant under an antiunitary antisymmetry: the anti-$\mathcal{PT}$ symmetry. The Hermitian Hamiltonians are defined on d-dimensional non-Bravais lattices. For an odd number of sublattices, the anti-$\mathcal{PT}$ symmetry protects a flatband at energy $E = 0$. We derive the anti-$\mathcal{PT}$ constraints on the Hamiltonian and use them to generate examples of generalized kagome networks in two and three lattice dimensions. Furthermore, we show that the anti-$\mathcal{PT}$ symmetry persists in the presence of uniform DC fields and ensures the presence of flatbands in the corresponding irreducible Wannier-Stark band structure. We provide examples of the Wannier-Stark band structure of generalized kagome networks in the presence of DC fields, and their implementation using Floquet engineering.

DOI: 10.1103/PhysRevA.105.L021305

Introduction. Flatband systems with single-particle dispersionless bands in their band structure [1–8] are important and promising platforms for exploring exotic phases and unconventional orders, due to the combined effect of macroscopic degeneracy of flatbands and applied perturbations. Possible perturbations include disorder [9–11], nonlinear interactions [10,12], and various many-body interactions [13–17]. The presence of localized eigenstates of a flatband are argued to be useful for quantum information storage and transfer [18–20] and for observing memory effects [21]. Remarkably, the presence of a uniform DC field leads to a Wannier-Stark (WS) ladder of $(d-1)$-dimensional irreducible band structures in a d-dimensional lattice. These irreducible band structures can again contain flatbands [22,23]. Being fine-tuned by nature, finding flatband Hamiltonians is in general a challenging problem. Multiple methods were developed to generate flatbands in translationally invariant systems that are based on fine-tuning [5,24,25], line graphs [26], origami rules [27], repetition of miniarrays [28], and application of magnetic field [6,29–31].

Flatbands can also emerge as a consequence of a symmetry. Local and latent symmetries have been shown to generate flatbands [32,33]. The other class of symmetries are global symmetries of the Hamiltonian. A global symmetry is associated with a symmetry operator Γ which is either unitary or antiunitary. A single-particle Hamiltonian $\mathcal{H}$ is antisymmetric if the following relation holds: $\Gamma \cdot \mathcal{H} \cdot \Gamma^{-1} = -\mathcal{H}$. The antisymmetry implies that for each eigenvalue E with eigenvector $|\psi_E\rangle$ there exists the negative eigenvalue $-E$ with eigenvector $\Gamma\,|\psi_E\rangle$. If the total number of eigenvalues is odd, it follows that at least one of them is zero. Translationally invariant lattice Hamiltonians are characterized by the number of their sublattices. Transforming the Hamiltonian into Bloch momentum space and observing $\Gamma(\vec{k}) \cdot \mathcal{H}(\vec{k}) \cdot \Gamma^{-1}(\vec{k}) = -\mathcal{H}(\vec{k})$ results in a macroscopically degenerated symmetry-protected $E = 0$ flatband for an odd number of sublattices.

One such example is the chiral symmetry that is realized by a unitary operator Γ. The chiral Hamiltonian in momentum space turns bipartite, $\mathcal{H}(\vec{k}) = \begin{pmatrix} \mathbb{O} & \mathbb{T}(\vec{k}) \\ \mathbb{T}^\dagger(\vec{k}) & \mathbb{O} \end{pmatrix}$, where $\mathbb{O}$ is a null matrix and $\mathbb{T}(\vec{k})$ is a rectangular matrix. Chiral flatband models and exhausting flatband generators have been reported for dimension $d = 1, 2, 3$ [34–36].

In this Letter, we explore the other possibility when the symmetry operator Γ is antiunitary and analyze the effect of the applied DC field. Only few results are known in this case. In $d = 2$, Green *et al.* [37] introduced a family of modified kagome lattices with three sublattices with nonzero local flux distributions which have a symmetry-protected flatband at energy $E = 0$ despite the breaking of time-reversal symmetry. Specific members of this modified kagome family were reported in later publications as well [38,39]. A specific decoration of the 2D Lieb lattice was also reported to feature a symmetry-protected flatband [40]. We note that all of the respective antiunitary operators $\Gamma = \mathcal{A}$ consist of a spatial point reflection (inversion through a point) in lattice position space $\mathcal{P}$, followed by a time-reversal operation $\mathcal{T}$ (usually simply an antilinear complex conjugation operation in lattice position basis): $\mathcal{A} = \mathcal{T} \cdot \mathcal{P}$. Therefore, all of the above examples enjoy anti-$\mathcal{PT}$ Hamiltonians.

When a commensurate uniform DC field [23] is applied, the band structure of the original d-dimensional Hamiltonian is modified into a WS ladder of irreducible $(d-1)$-dimensional band structures with the same number of bands [41]. The particular case of the 2D dice lattice with three bands resulted in a WS flatband in the presence of a

*marindam@ibs.re.kr
†nnchangqq@gmail.com
‡aalexei@ibs.re.kr
§sflach@ibs.re.kr

 ©2022 American Physical Society

DC field, which was believed to be protected by the chiral (bipartite) symmetry of the original dice lattice [22]. However, this symmetry appears to be lost in the presence of DC fields, and the flatband existence proof in Ref. [22] does not explicitly rely on it. However, we note that the dice lattice is also invariant under anti-$\mathcal{PT}$ symmetry. As we show below, this symmetry remains, in general, intact in the presence of a nonzero DC field.

We derive the constraints for a general Hermitian Hamiltonian $\mathcal{H}$ on a d-dimensional non-Bravais lattice to be anti-$\mathcal{PT}$ symmetric:

$$\mathcal{A}\cdot\mathcal{H}\cdot\mathcal{A}^{-1}=-\mathcal{H}. \tag{1}$$

The anti-$\mathcal{PT}$ symmetry condition and an odd number of sublattices are sufficient to protect at least one flatband—both in the absence and presence of DC fields.

Definitions. We consider a Hermitian tight-binding Hamiltonian on a d-dimensional non-Bravais lattice. Every lattice site is labeled by its unit cell index vector $\vec{n}=\sum_{j=1}^{d} n_j\vec{a}_j$ and sublattice index $\nu=1,2,\ldots,\mu$. The numbers n_j are integers and $\vec{a}_j$ are d-dimensional unit cell basis vectors (and are, in general, neither orthogonal nor normalized). Similar to the lattice vector $\vec{n}$, we define the sublattice vectors $\vec{m}_\nu=\sum_{i=1}^{d} m_{\nu,i}\vec{a}_i$ which locate sublattice sites relative to a unit cell: $-1<m_{\nu,i}<1$. Consequently, we label the Hilbert space basis vectors as $|\nu,\vec{n}\rangle$. The single-particle translationally invariant Hamiltonian reads

$$\mathcal{H}=-\sum_{\vec{l},\vec{n}}\sum_{\nu,\sigma=1}^{\mu} t_{\nu,\sigma}(\vec{l})|\nu,\vec{n}\rangle\langle\sigma,\vec{n}+\vec{l}|. \tag{2}$$

The hopping amplitude $t_{\nu,\sigma}(\vec{l})=t^{*}_{\sigma,\nu}(-\vec{l})$ connects site $(\sigma,\vec{n}+\vec{l})$ with site $(\nu,\vec{n})$. Application of the Bloch theorem on the Hamiltonian (2) block diagonalizes it in the quasimomentum basis $\{|\vec{k}\rangle\}$. Each block is a $\mu\times\mu$ matrix acting only on the sublattice space:

$$\mathcal{H}(\vec{k}):=-\sum_{\vec{l}}\sum_{\nu,\sigma=1}^{\mu} t_{\nu,\sigma}(\vec{l})e^{i\vec{k}\cdot\vec{l}}\,|\nu\rangle\,\langle\sigma|\,. \tag{3}$$

If μ is odd, an antisymmetry of the Hamiltonian $\mathcal{H}(\vec{k})$ results in a zero eigenvalue. If that antisymmetry holds for all $\vec{k}$, then the Hamiltonian possesses a zero-energy flatband.

The anti-$\mathcal{PT}$ symmetry operator reads

$$\mathcal{A}=\mathcal{T}\cdot\mathcal{P}=\mathcal{T}\cdot\sum_{\nu,\vec{n}} e^{i\xi_\nu}\,|f(\nu),-\vec{n}-\vec{p}_\nu\rangle\,\langle\nu,\vec{n}|\,. \tag{4}$$

The one-to-one map $f(\nu)$ describes the swap of the sublattice indices upon lattice point inversion. It is defined by the lattice geometry and it is its own inverse: $f^{-1}=f$. For instance, with three sublattices the only choices are $f_1:1\mapsto1,2\mapsto2,3\mapsto3$, and $f_2:1\mapsto1,2\mapsto3,3\mapsto2$ (up to a freedom of the sublattice index relabeling). The 2D Lieb and kagome lattices implement f_1, while the 2D dice lattice implements f_2. Inversion in position space results in inverting the sign of a unit cell vector $\vec{n}\mapsto-\vec{n}$. However, the inversion can map a given sublattice point of unit cell $\vec{n}$ into one of the neighboring cells of $-\vec{n}$. Therefore, we had to introduce the lattice vectors $\vec{p}_\nu$ in Eq. (4). $\vec{p}_\nu$ relates the sublattice vectors: $\vec{m}_\nu+\vec{m}_{f(\nu)}=\vec{p}_\nu$. The gauge phases ξ_ν relate to the magnetic flux distributions (if present) in the models of interest. Since we consider an odd number of sublattices, it follows that $\mathcal{A}^2=\mathbb{1}$ (see Supplemental Material [42] for details). This implies the following constraints: $\vec{p}_\nu=\vec{p}_{f(\nu)}$ and $\xi_\nu=\xi_{f(\nu)}$. For instance, in the case of three sublattices, f_1 allows for three independent gauge phases while f_2 allows for only two independent gauge phases. Combining Eqs. (1) and (4), we arrive at the following constraints on the hoppings for an anti-$\mathcal{PT}$ symmetric Hamiltonian (2):

$$e^{-i\xi_\nu+i\xi_\sigma}t^{*}_{\nu,\sigma}(\vec{l})=-t_{f(\nu),f(\sigma)}(-\vec{l}+\vec{p}_\nu-\vec{p}_\sigma). \tag{5}$$

The above constraint on the hoppings can be used to efficiently construct anti-$\mathcal{PT}$ symmetric Hamiltonians. For a single sublattice (e.g., a Bravais lattice) the above condition (5) reduces to $t^{*}(\vec{l})=-t(-\vec{l})$. At the same time, the Hermiticity of the Hamiltonian enforces $t^{*}(\vec{l})=t(-\vec{l})$. Both conditions can only be satisfied for the trivial case of no hopping $t(\vec{l})=0$. Therefore, the anti-$\mathcal{PT}$ symmetry requires two or more sublattices.

Anti-$\mathcal{PT}$ protected flatbands. Let us project both sides of Eq. (1) onto the $\vec{k}$ space:

$$\mathcal{A}(\vec{k})\cdot\mathcal{H}(\vec{k})\cdot\mathcal{A}(\vec{k})^{-1}=-\mathcal{H}(\vec{k}). \tag{6}$$

For a Hamiltonian satisfying Eq. (5), the anti-$\mathcal{PT}$ operator (4) transforms as

$$\mathcal{A}(\vec{k})=\mathcal{T}_s\cdot\sum_{\nu=1}^{\mu} e^{i\xi_\nu}e^{-i\vec{k}\cdot\vec{p}_\nu}|f(\nu)\rangle\langle\nu|, \tag{7}$$

where $\mathcal{T}_s$ is a complex conjugation operator and it acts only on the sublattice space. For an odd number of sublattices μ, one of the μ eigenvalues of $\mathcal{H}(\vec{k})$ is zero. As this is true for all $\vec{k}$, it follows that one of the bands must be flat with energy equal to zero.

In Fig. 1, we show an anti-$\mathcal{PT}$ symmetric generalized 2D kagome lattice with an $E=0$ flatband compatible with Eq. (5). The sublattice vectors are $\vec{m}_1=\frac{1}{2}\vec{a}_2$, $\vec{m}_2=\vec{0}$, and $\vec{m}_3=\frac{1}{2}\vec{a}_1$, while $f(\nu)=\nu$, $\vec{p}_1=\vec{a}_2$, $\vec{p}_2=\vec{0}$, and $\vec{p}_3=\vec{a}_1$. The hopping parameters are detailed in the caption of Fig. 1. Diagonalizing the Hamiltonian $\mathcal{H}(\vec{k})$ for this choice of parameters, we obtain three bands (see Supplemental Material [42]).

The anti-$\mathcal{PT}$ band structure is shown in Fig. 1(b). The anti-$\mathcal{PT}$ flatband supports eigenstates which are compact localized states (CLSs) occupying three unit cells as shown in Fig. 1(a). The CLS amplitudes up to normalization are $\equiv-t$ (black diamonds), $\equiv e^{i\varphi}$ (black filled circle), $\equiv e^{-i\varphi}$ (empty big circle), $\equiv+1$ (black filled square), and $\equiv-1$ (empty square).

To arrive at a 3D version of the kagome lattice, shown in Fig. 2(d), we stack the 2D kagome lattices shown in Fig. 1(a) on top of each other vertically with $|\vec{a}_3|=1$. Two additional hoppings connect neighboring 2D kagome planes: $t_{1,2}(0,0,1)=2$ and $t_{1,2}(0,1,-1)=2$. The spectrum is now a function of three reciprocal momenta (k_1,k_2,k_3). In Figs. 2(a)–(c), we plot three different 3D intersections of the band structure $E(k_1,k_2,k_3)$. All of them contain an anti-$\mathcal{PT}$ flatband at zero energy.

Anti-$\mathcal{PT}$ protected Wannier-Stark flatbands. We now outline and prove the survival of the anti-$\mathcal{PT}$ symmetry in the

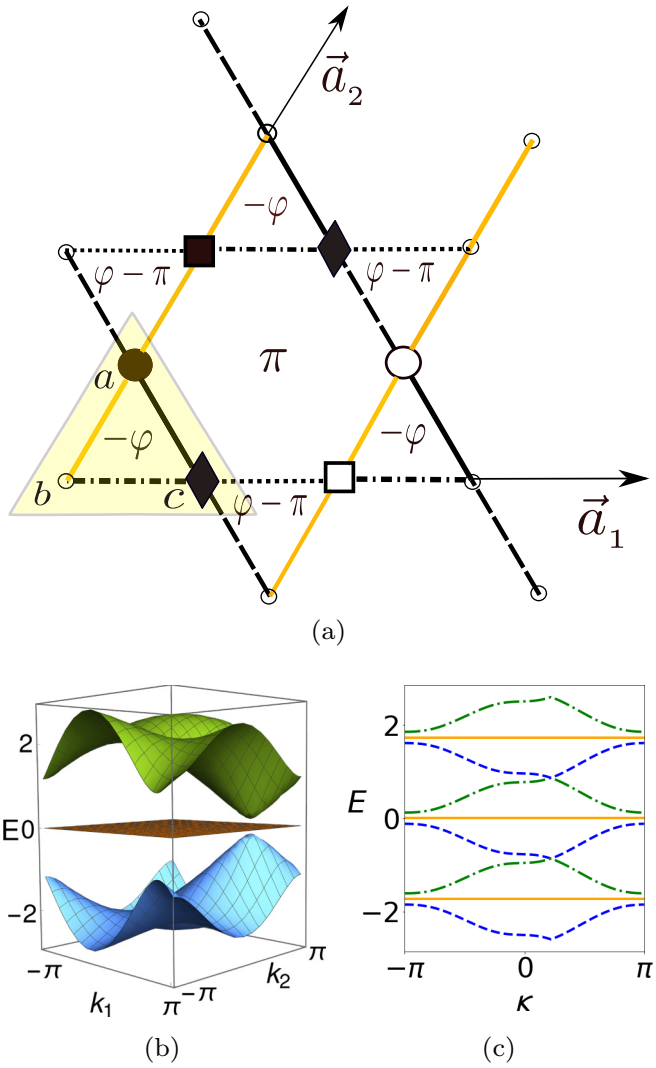

FIG. 1. (a) The anti-$\mathcal{PT}$ symmetric generalized 2D kagome lattice. The lattice sites are shown by small empty black circles. A single unit cell is shown within a shaded triangle with the sublattice sites a ($\nu = 1$), b ($\nu = 2$), and c ($\nu = 3$). The hoppings $t_{3,1}(1,-1) = -1$ (black dashed lines), $t_{2,3}(0,0) = e^{i\varphi}$ (black dashed-dotted lines), $t_{2,3}(-1,0) = e^{-i\varphi}$ (black dotted lines), $t_{1,2}(0,1) = t_{1,2}(0,0) = t$ (yellow solid lines), $t_{1,3}(0,0) = 1$ (solid black lines). The fluxes φ induced by anti-$\mathcal{PT}$ symmetric complex hopping choices are denoted inside each plaquette, with all fluxes computed counterclockwise. The compact localized eigenstate at the anti-$\mathcal{PT}$ flatband energy $E = 0$ has nonzero wave-function amplitudes indicated by large circles, diamonds, and squares (for more details, we refer to the main text). (b) Band structure $E(k_1, k_2)$ for $\varphi = \frac{\pi}{5}$ and $t = 0.15$. (c) Three subsequent irreducible Wannier-Stark band structures computed using Eq. (16) for the DC field direction $\vec{a}_1 + \vec{a}_2$. The field strength $|\vec{\mathcal{E}}| = 2$.

presence of a uniform DC field $\vec{\mathcal{E}}$ for an anti-$\mathcal{PT}$ symmetric Hamiltonian. The DC field adds an on-site potential term in the Hamiltonian (2) and the full Hamiltonian reads

$$\mathcal{H}_{\mathcal{E}} = \vec{\mathcal{E}} \cdot \hat{r} + \mathcal{H}. \tag{8}$$

Here we defined the lattice position operator as $\hat{r} = \sum_{\nu,\vec{n}} (\vec{n} + \vec{m}_\nu) |\nu, \vec{n}\rangle \langle \nu, \vec{n}|$. The DC field term $\vec{\mathcal{E}} \cdot \hat{r}$ changes signs under

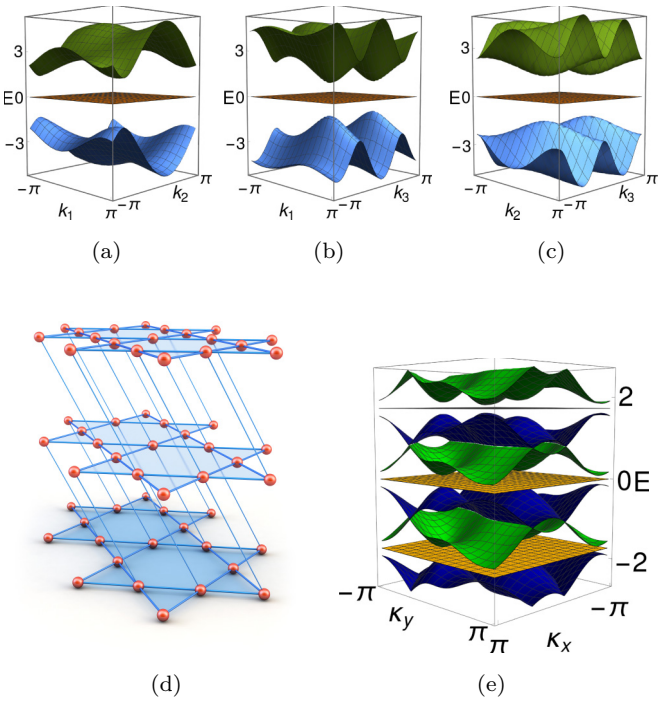

FIG. 2. The anti-$\mathcal{PT}$ symmetric generalized 3D kagome lattice. (a)–(c) Three constrained band structures: (a) $E(k_1, k_2, k_3 = \frac{\pi}{7})$, (b) $E(k_1, k_2 = \frac{\pi}{7}, k_3)$, (c) $E(k_1 = \frac{\pi}{7}, k_2, k_3)$. (d) The lattice structure. The sites are denoted by small solid red spheres. The hopping connections within each 2D kagome plane are the same as in Fig. 1(b). The intraplane hoppings $t_{1,2}(0,0,1) = 2$ and $t_{1,2}(0,1,-1) = 2$. (e) Three subsequent irreducible Wannier-Stark band structures $E_{\gamma,a}(\kappa_x, \kappa_y)$ computed using Eq. (16) for the field direction $(2,2,3) \equiv 2\vec{a}_1 + 2\vec{a}_2 + 3\vec{a}_3$. The field strength $|\vec{\mathcal{E}}| = \sqrt{7}$.

the application of the anti-$\mathcal{PT}$ operator $\mathcal{A}$ due to lattice reflection $\mathcal{P}$: $(\vec{n} + \vec{m}_\nu) \mapsto -(\vec{n} + \vec{m}_\nu)$. Together with condition (5), this ensures

$$\mathcal{A} \cdot \mathcal{H}_{\mathcal{E}} \cdot \mathcal{A}^{-1} = -\mathcal{H}_{\mathcal{E}}. \tag{9}$$

The application of the uniform DC field breaks translation invariance and eliminates the band structure for generic directions of the DC field. However, for special field directions, translation invariance is broken only partially and a WS band structure emerges as translation invariance is preserved in the direction orthogonal to the field. We refer to such field directions as *commensurate* [23]. The unit cell and sublattice coordinates along the field, z and z_ν, respectively, are defined as $z = \frac{1}{\mathcal{F}} \vec{\mathcal{E}} \cdot \vec{n}$, $z_\nu = \frac{1}{\mathcal{F}} \vec{\mathcal{E}} \cdot \vec{m}_\nu$ with the scaling factor $\mathcal{F}$ ensuring that z taking integer values. The directions perpendicular to $\vec{\mathcal{E}}$ are parameterized by a $d-1$ dimensional integer vector $\vec{\eta}$ (see Supplemental Material [42] for details). The Hamiltonian $\mathcal{H}_{\mathcal{E}}$ is translationally invariant in $\vec{\eta}$. With the use of the Bloch basis for $\vec{\eta}$,

$$|\psi_E(\vec{\kappa})\rangle = (2\pi)^{\frac{1-d}{2}} \sum_{z,\nu,\vec{\eta}} \psi_E(\nu, z, \vec{\kappa}) e^{i\vec{\kappa}\cdot\vec{\eta}} |\nu, z, \vec{\eta}\rangle, \tag{10}$$

the Hamiltonian (8) becomes block diagonal:

$$\mathcal{H}_{\mathcal{E}} = \int_{\vec{\kappa}} \mathcal{H}_{\mathcal{E}}(\vec{\kappa}) d\vec{\kappa}, \quad \mathcal{H}_{\mathcal{E}}(\vec{\kappa})\,|\psi_E(\vec{\kappa})\rangle = E(\vec{\kappa})\,|\psi_E(\vec{\kappa})\rangle\,. \tag{11}$$

Each block is infinite dimensional due to the coupling along the z direction. The commensurability condition for the DC field implies the persistence of a generalized translational invariance along the field direction, which goes along with an overall shift of the eigenenergies. Following Refs. [22,23], we Fourier transform from z space to its conjugate momentum q space $\vec{g}_E(q,\vec{\kappa}) = (2\pi)^{-1/2} e^{\frac{-iEq}{\mathcal{F}}} \sum_{z,\nu} e^{iq(z+z_\nu)} \psi_E(\nu, z, \vec{\kappa})\,|\nu\rangle$ to arrive at μ coupled differential equations (see Supplemental Material [42] for derivation):

$$i\frac{\partial}{\partial q}\vec{g}_E(q,\vec{\kappa}) = \mathcal{H}_{\mathcal{E}}(q,\vec{\kappa})\vec{g}_E(q,\vec{\kappa}). \tag{12}$$

The resulting Hermitian Hamiltonian

$$\mathcal{H}_{\mathcal{E}}(q,\vec{\kappa}) = -\frac{1}{\mathcal{F}} \sum_{\vec{l},\nu,\sigma} t_{\nu,\sigma}(\vec{l})\,|\nu\rangle\,\langle\sigma|\, e^{iq(z_\nu - z_\sigma)} e^{i\vec{\kappa}\cdot\vec{\epsilon}(\vec{l}) - \frac{iq\vec{\mathcal{E}}\cdot\vec{l}}{\mathcal{F}}} \tag{13}$$

is a $\mu \times \mu$ matrix which acts on the sublattice space $\{|\nu\rangle\}$ only, $\vec{\epsilon}(\vec{l})$ is the hopping perpendicular to the field. Equation (12) describes a unitary evolution of $\vec{g}_E(q,\vec{\kappa})$ in q space,

$$\vec{g}_E(q,\vec{\kappa}) = U(q,\vec{\kappa})\cdot\vec{g}_E(0,\vec{\kappa}), \tag{14}$$

where $U(q,\vec{\kappa})$ is a q-ordered exponential of the integrated $\mathcal{H}_{\mathcal{E}}(q,\vec{\kappa})$:

$$U(q,\vec{\kappa}) = \mathbb{1} + (-i)\int_{q'=0}^{q} dq' \mathcal{H}_{\mathcal{E}}(q',\vec{\kappa}) + (-i)^2 \int_{q'=0}^{q} \times \int_{q''=0}^{q'} dq' dq'' \mathcal{H}_{\mathcal{E}}(q',\vec{\kappa})\mathcal{H}_{\mathcal{E}}(q'',\vec{\kappa}) + \cdots. \tag{15}$$

By construction, $\vec{g}_E(2\pi,\vec{\kappa}) = e^{-\frac{2\pi i E}{\mathcal{F}}}\Lambda(2\pi)\cdot\vec{g}_E(0,\vec{\kappa})$, where the matrix $\Lambda(q)$ is diagonal with entries $\Lambda_{\nu\nu}(q) = e^{iqz_\nu}$. Then, from Eq. (14) and the above periodicity condition, we arrive at the eigenvalue problem on the WS bands:

$$[\Lambda^\dagger(2\pi)\cdot U(2\pi,\vec{\kappa})]\cdot\vec{g}_E(0,\vec{\kappa}) = e^{-\frac{2\pi i E}{\mathcal{F}}}\vec{g}_E(0,\vec{\kappa}). \tag{16}$$

The spectrum of $\mathcal{H}_{\mathcal{E}}$ is obtained by solving the above eigenproblem,

$$E \equiv E_{\gamma,a}(\vec{\kappa}) = \mathcal{F}a + \frac{i\mathcal{F}}{2\pi}\ln[\lambda_\gamma(\vec{\kappa})], \tag{17}$$

where $a \in \mathbb{Z}$ and λ_γ are the eigenvalues of the $\mu \times \mu$ unitary matrix $\Lambda^\dagger(2\pi)\cdot U(2\pi,\vec{\kappa})$. The irreducible WS band structure is obtained by choosing a particular value of a, e.g., $a = 0$. The entire spectrum is generated by a parallel shift of the irreducible band structure and is parameterized by the band indices (γ, a).

We now arrive at the formulation of our anti-$\mathcal{PT}$ *theorem* in the presence of the commensurate DC field: *If the original Hamiltonian $\mathcal{H}$ has an odd number of sublattices and is anti-$\mathcal{PT}$ symmetric, the irreducible WS band structure of $\mathcal{H}_{\mathcal{E}}$ contains at least one flatband.*

Proof: Indeed, the anti-$\mathcal{PT}$ condition (9) translates into a similar condition for the effective Hamiltonian $\mathcal{H}_{\mathcal{E}}(q,\vec{\kappa})$,

$$\mathcal{H}^*_{\mathcal{E}}(q,\vec{\kappa}) = -\mathcal{M}^\dagger(\vec{\kappa})\cdot\mathcal{H}_{\mathcal{E}}(q,\vec{\kappa})\cdot\mathcal{M}(\vec{\kappa}), \tag{18}$$

where the $\mu \times \mu$ unitary matrix

$$\mathcal{M}(\vec{\kappa}) = \sum_\nu e^{-i\xi_\nu} e^{i\vec{\kappa}\cdot\vec{\epsilon}(\vec{p}_\nu)}\,|f(\nu)\rangle\,\langle\nu|\,. \tag{19}$$

$\vec{\epsilon}(\vec{p}_\nu)$ is the same vector function of $\vec{l}$ as in Eq. (13) but its argument is replaced by $\vec{p}_\nu$. Then, from Eq. (15) it is straightforward to establish that

$$U^*(q,\vec{\kappa}) = \mathcal{M}^\dagger(\vec{\kappa})\cdot U(q,\vec{\kappa})\cdot\mathcal{M}(\vec{\kappa}). \tag{20}$$

We note that by definition of the commensurate DC field direction, the projection of $\vec{p}_\nu$ along the field direction will be an integer and hence $(z_\nu + z_{f(\nu)})$ will be an integer as well (see Supplemental Material [42] for details). Therefore, $e^{2\pi i(z_\nu + z_{f(\nu)})} = 1$. Since the operator $\mathcal{M}(\vec{\kappa})$ maps the sublattice vector $|\nu\rangle$ to $|f(\nu)\rangle$, it follows that

$$\Lambda^\dagger(2\pi) = \mathcal{M}(\vec{\kappa})\cdot\Lambda(2\pi)\cdot\mathcal{M}^\dagger(\vec{\kappa}). \tag{21}$$

We use the relations (20) and (21) to rewrite the eigenvalue problem (16) into the following form (see Supplmental Material [42]):

$$[\Lambda^\dagger(2\pi)\cdot U(2\pi,\vec{\kappa})]\cdot[\mathcal{M}(\vec{\kappa})\cdot\vec{g}^*_E(0,\vec{\kappa})] = e^{\frac{2\pi i E}{\mathcal{F}}}[\mathcal{M}(\vec{\kappa})\cdot\vec{g}^*_E(0,\vec{\kappa})]. \tag{22}$$

Equations (16) and (22) imply that the eigenvalues of the unitary operator $[\Lambda^\dagger(2\pi)\cdot U(2\pi,\vec{\kappa})]$ come in pairs $(e^{-\frac{2\pi i E(\vec{\kappa})}{\mathcal{F}}}, e^{\frac{2\pi i E(\vec{\kappa})}{\mathcal{F}}})$. For an odd number of sublattices μ, the number of eigenvalues of the operator $[\Lambda^\dagger(2\pi)\cdot U(2\pi,\vec{\kappa})]$ is also odd. Therefore, at least one eigenvalue satisfies $e^{-\frac{2\pi i E(\vec{\kappa})}{\mathcal{F}}} = e^{\frac{2\pi i E(\vec{\kappa})}{\mathcal{F}}}$ with $E(\vec{\kappa})$ being $\vec{\kappa}$ independent and a multiple of $\frac{\mathcal{F}}{2}$. Therefore, the irreducible WS band structure contains at least one anti-$\mathcal{PT}$ symmetry protected flatband. □

We check the validity of the above theorem by computing WS band structures with (16) for the 2D kagome lattice in Fig. 1 and 3D kagome lattice in Fig. 2. Details on the field direction and strength are provided in the corresponding captions. We observe and confirm the presence of anti-$\mathcal{PT}$ protected WS flatbands in Fig. 1(c) for the 2D case and in Fig. 2(e) for the 3D case.

Experimental realizations. Flatband models have already been designed in metallic systems [43], photonic lattices [44–49], and ultracold atoms in optical lattices [50]. The unperturbed kagome lattices introduced above can be tested in similar setups [44,50] by proper design of hopping parameters with artificial gauge fields.

To observe the WS effect in optical lattices with ultracold atomic gases, they can be tilted, so the gravitational field acts as a DC field source [51]. Moreover, one can study the impact of an electric DC field on centrosymmetric lattices as reported in a very recent experiment on diamond [52]. Another option for implementing the WS Hamiltonians is to use Floquet engineering following recent experiments, which implemented Floquet Hamiltonians using ultracold atoms [53,54]. The spectrum of WS Hamiltonians can be

mapped onto that of periodically driven systems [55] and vise versa. Mapping the frequency space of a Floquet $(d-1)$-dimensional lattice Hamiltonian to a new spatial dimension produces an effective static Hamiltonian in a d-dimensional lattice with WS potential. In this case, the single set of Floquet bands, which are periodic in energy, unfolds into an infinitely repeated tower of WS bands. The details of the mapping between our WS Hamiltonians in 2D (3D) kagome networks and the Hamiltonians having Floquet Peierls phases in 1D (2D) diamond lattices are provided in the Supplemental Material [42].

Discussion and conclusions. We considered tight-binding lattice Hamiltonians on d-dimensional non-Bravais lattices, which are invariant under the anti-$\mathcal{PT}$ symmetry. We proved that the anti-$\mathcal{PT}$ symmetry protects a flatband at energy $E = 0$ for odd numbers of sublattices. We derived the precise anti-$\mathcal{PT}$ constraints on the Hamiltonian and used them to generate examples of generalized kagome networks. Remarkably the anti-$\mathcal{PT}$ symmetry persists in the presence of uniform DC fields. We prove that the corresponding irreducible WS band structures will again contain anti-$\mathcal{PT}$ protected flatbands. We demonstrate the validity of our results by computing examples of the WS band structure of generalized 2D and 3D kagome networks in the presence of DC fields.

The zero-energy flatbands reported in Refs. [37–40] belong to the anti-$\mathcal{PT}$ class. They were reported for specific choices of hoppings for two-dimensional lattices. Our results also explain the persistence of the flatband in the dice lattice [22] in the presence of the DC field. The original proof relied on specific properties of the hopping network, and subsequent conjectures attempted to connect the proof to the bipartiteness of the unbiased lattice. Actually, the unbiased dice lattice is both chiral and anti-$\mathcal{PT}$ symmetric. Therefore, its $E = 0$ flatband is protected by both the chiral and the anti-$\mathcal{PT}$ symmetries. Adding a DC field destroys the chiral symmetry but preserves the anti-$\mathcal{PT}$ symmetry. Therefore, the emerging WS flatbands in the irreducible WS band structure are protected by the anti-$\mathcal{PT}$ symmetry. Anti-$\mathcal{PT}$ networks do not need to be bipartite and our proof is valid for any d-dimension with arbitrary number of sublattices.

Our study focused on spinless single particle translationally invariant Hermitian Hamiltonians on non-Bravais lattices. Our results also apply to a particle with an integer spin (or other internal degrees of freedom, e.g., orbital degrees of freedom) including spin-orbit coupling on a Bravais lattice. The impact of disorder, many-body interactions, nonlinearities, or non-Hermiticity on our system are possible interesting directions for future investigations. We expect that methods developed to analyze the impact of these perturbations for other flatband models might be helpful in our setting as well. It is also interesting to study the case of incommensurate DC field directions that are expected to generate quasicrystalline structures.

Acknowledgments. This work was supported by Institute for Basic Science in Korea (No. IBS-R024-D1). N.C. acknowledges financial support from the China Scholarship Council (No. CSC-201906040021). We thank Jung-Wan Ryu for helpful discussions.

[1] S. Flach, D. Leykam, J. D. Bodyfelt, P. Matthies, and A. S. Desyatnikov, Detangling flatbands into Fano lattices, Europhys. Lett. **105**, 30001 (2014).

[2] O. Derzhko, J. Richter, and M. Maksymenko, Strongly correlated flat-band systems: The route from Heisenberg spins to Hubbard electrons, Int. J. Mod. Phys. B **29**, 1530007 (2015).

[3] D. Leykam, A. Andreanov, and S. Flach, Artificial flat band systems: From lattice models to experiments, Adv. Phys. X **3**, 1473052 (2018).

[4] D. Leykam and S. Flach, Perspective: Photonic flatbands, APL Photonics **3**, 070901 (2018).

[5] W. Maimaiti, A. Andreanov, H. C. Park, O. Gendelman, and S. Flach, Compact localized states and flat-band generators in one dimension, Phys. Rev. B **95**, 115135 (2017).

[6] R. Khomeriki and S. Flach, Landau-Zener Bloch Oscillations with Perturbed Flatbands, Phys. Rev. Lett. **116**, 245301 (2016).

[7] J.-W. Rhim, K. Kim, and B.-J. Yang, Quantum distance and anomalous Landau levels of flatbands, Nature (London) **584**, 59 (2020).

[8] J.-W. Rhim and B.-J. Yang, Singular flat bands, Adv. Phys.: X **6**, 1901606 (2021).

[9] M. Goda, S. Nishino, and H. Matsuda, Inverse Anderson Transition caused by Flatbands, Phys. Rev. Lett. **96**, 126401 (2006).

[10] D. Leykam, S. Flach, O. Bahat-Treidel, and A. S. Desyatnikov, Flatband states: Disorder and nonlinearity, Phys. Rev. B **88**, 224203 (2013).

[11] N. Roy, A. Ramachandran, and A. Sharma, Interplay of disorder and interactions in a flat-band supporting diamond chain, Phys. Rev. Research **2**, 043395 (2020).

[12] C. Danieli, A. Andreanov, T. Mithun, and S. Flach, Nonlinear caging in all-bands-flat lattices, Phys. Rev. B **104**, 085131 (2021).

[13] Y. Kuno, T. Mizoguchi, and Y. Hatsugai, flatband quantum scar, Phys. Rev. B **102**, 241115(R) (2020).

[14] C. Danieli, A. Andreanov, T. Mithun, and S. Flach, Quantum caging in interacting many-body all-bands-flat lattices, Phys. Rev. B **104**, 085132 (2021).

[15] T. T. Heikkilä and G. E. Volovik, Flat bands as a route to high-temperature superconductivity in graphite, in *Basic Physics of Functionalized Graphite*, edited by P. Esquinazi, Springer Series in Materials Science, Vol. 244 (Springer, Cham, 2016), pp. 123–143.

[16] L. H. C. M. Nunes and C. M. Smith, Flat-band superconductivity for tight-binding electrons on a square-octagon lattice, Phys. Rev. B **101**, 224514 (2020).

[17] T. Orito, Y. Kuno, and I. Ichinose, Nonthermalized dynamics of flat-band many-body localization, Phys. Rev. B **103**, L060301 (2021).

[18] M. Röntgen, C. V. Morfonios, I. Brouzos, F. K. Diakonos, and P. Schmelcher, Quantum Network Transfer and Storage with Compact Localized States Induced by Local Symmetries, Phys. Rev. Lett. **123**, 080504 (2019).

[19] S. Taie, T. Ichinose, H. Ozawa, and Y. Takahashi, Spatial adiabatic passage of massive quantum particles in an optical Lieb lattice, Nat. Commun. **11**, 257 (2020).
[20] M. Röntgen, N. Palaiodimopoulos, C. Morfonios, I. Brouzos, M. Pyzh, F. Diakonos, and P. Schmelcher, Designing pretty good state transfer via isospectral reductions, Phys. Rev. A **101**, 042304 (2020).
[21] C.-Y. Lai and C.-C. Chien, Geometry-Induced Memory Effects in Isolated Quantum Systems: Cold-Atom Applications, Phys. Rev. Appl. **5**, 034001 (2016).
[22] A. R. Kolovsky, A. Ramachandran, and S. Flach, Topological flat Wannier-Stark bands, Phys. Rev. B **97**, 045120 (2018).
[23] A. Mallick, N. Chang, W. Maimaiti, S. Flach, and A. Andreanov, Wannier-Stark flatbands in Bravais lattices, Phys. Rev. Research **3**, 013174 (2021).
[24] W. Maimaiti, S. Flach, and A. Andreanov, Universal $d = 1$ flatband generator from compact localized states, Phys. Rev. B **99**, 125129 (2019).
[25] W. Maimaiti, A. Andreanov, and S. Flach, Flat-band generator in two dimensions, Phys. Rev. B **103**, 165116 (2021).
[26] A. Mielke, Ferromagnetism in the Hubbard model on line graphs and further considerations, J. Phys. A: Math. Gen. **24**, 3311 (1991).
[27] R. Dias and J. Gouveia, Origami rules for the construction of localized eigenstates of the Hubbard model in decorated lattices, Sci. Rep. **5**, 16852 (2015).
[28] L. Morales-Inostroza and R. A. Vicencio, Simple method to construct flat-band lattices, Phys. Rev. A **94**, 043831 (2016).
[29] M. Creutz, End States, Ladder Compounds, and Domain-Wall Fermions, Phys. Rev. Lett. **83**, 2636 (1999).
[30] G. Möller and N. R. Cooper, Synthetic gauge fields for lattices with multi-orbital unit cells: Routes towards a π-flux dice lattice with flatbands, New J. Phys. **20**, 073025 (2018).
[31] D. Yu, L. Yuan, and X. Chen, Isolated photonic flatband with the effective magnetic flux in a synthetic space including the frequency dimension, Laser Photonics Rev. **14**, 2000041 (2020).
[32] M. Röntgen, C. V. Morfonios, and P. Schmelcher, Compact localized states and flatbands from local symmetry partitioning, Phys. Rev. B **97**, 035161 (2018).
[33] C. V. Morfonios, M. Röntgen, M. Pyzh, and P. Schmelcher, Flatbands by latent symmetry, Phys. Rev. B **104**, 035105 (2021).
[34] B. Sutherland, Localization of electronic wave functions due to local topology, Phys. Rev. B **34**, 5208 (1986).
[35] J. Mur-Petit and R. A. Molina, Chiral bound states in the continuum, Phys. Rev. B **90**, 035434 (2014).
[36] A. Ramachandran, A. Andreanov, and S. Flach, Chiral flatbands: Existence, engineering, and stability, Phys. Rev. B **96**, 161104(R) (2017).
[37] D. Green, L. Santos, and C. Chamon, Isolated flatbands and spin-1 conical bands in two-dimensional lattices, Phys. Rev. B **82**, 075104 (2010).
[38] J. Koch, A. A. Houck, K. L. Hur, and S. M. Girvin, Time-reversal-symmetry breaking in circuit-qed-based photon lattices, Phys. Rev. A **82**, 043811 (2010).
[39] C. Wei and T. A. Sedrakyan, Optical lattice platform for the Sachdev-Ye-Kitaev model, Phys. Rev. A **103**, 013323 (2021).
[40] L. Chen, T. Mazaheri, A. Seidel, and X. Tang, The impossibility of exactly flat non-trivial Chern bands in strictly local periodic tight binding models, J. Phys. A: Math. Theor. **47**, 152001 (2014).
[41] D. N. Maksimov, E. N. Bulgakov, and A. R. Kolovsky, Wannier-Stark states in double-periodic lattices. II. Two-dimensional lattices, Phys. Rev. A **91**, 053632 (2015).
[42] See Supplemental Material at http://link.aps.org/supplemental/10.1103/PhysRevA.105.L021305 for rigorous mathematical details of our theory.
[43] S. Kajiwara, Y. Urade, Y. Nakata, T. Nakanishi, and M. Kitano, Observation of a nonradiative flatband for spoof surface plasmons in a metallic Lieb lattice, Phys. Rev. B **93**, 075126 (2016).
[44] Y. Zong, S. Xia, L. Tang, D. Song, Y. Hu, Y. Pei, J. Su, Y. Li, and Z. Chen, Observation of localized flat-band states in kagome photonic lattices, Opt. Express **24**, 8877 (2016).
[45] S. Mukherjee and R. R. Thomson, Observation of robust flat-band localization in driven photonic rhombic lattices, Opt. Lett. **42**, 2243 (2017).
[46] S. Xia, Y. Hu, D. Song, Y. Zong, L. Tang, and Z. Chen, Demonstration of flat-band image transmission in optically induced Lieb photonic lattices, Opt. Lett. **41**, 1435 (2016).
[47] S. Xia, C. Danieli, W. Yan, D. Li, S. Xia, J. Ma, H. Lu, D. Song, L. Tang, S. Flach, and Z. Chen, Observation of quincunx-shaped and dipole-like flatband states in photonic rhombic lattices without band-touching, APL Photonics **5**, 016107 (2020).
[48] W. Yan, H. Zhong, D. Song, Y. Zhang, S. Xia, L. Tang, D. Leykam, and Z. Chen, Flatband line states in photonic super-honeycomb lattices, Adv. Opt. Mater. **8**, 1902174 (2020).
[49] L. Tang, D. Song, S. Xia, S. Xia, J. Ma, W. Yan, Y. Hu, J. Xu, D. Leykam, and Z. Chen, Photonic flat-band lattices and unconventional light localization, Nanophotonics **9**, 1161 (2020).
[50] G.-B. Jo, J. Guzman, C. K. Thomas, P. Hosur, A. Vishwanath, and D. M. Stamper-Kurn, Ultracold Atoms in a Tunable Optical Kagome Lattice, Phys. Rev. Lett. **108**, 045305 (2012).
[51] B. Anderson and M. Kasevich, Macroscopic quantum interference from atomic tunnel arrays, Science **282**, 1686 (1998).
[52] L. De Santis, M. E. Trusheim, K. C. Chen, and D. R. Englund, Investigation of the Stark Effect on a Centrosymmetric Quantum Emitter in Diamond, Phys. Rev. Lett. **127**, 147402 (2021).
[53] P. Bordia, H. Lüschen, U. Schneider, M. Knap, and I. Bloch, Periodically driving a many-body localized quantum system, Nat. Phys. **13**, 460 (2017).
[54] A. Eckardt, Colloquium: Atomic quantum gases in periodically driven optical lattices, Rev. Mod. Phys. **89**, 011004 (2017).
[55] T. Oka and S. Kitamura, Floquet engineering of quantum materials, Annu. Rev. Condens. Matter Phys. **10**, 387 (2019).